DOE/ER/45167--T1

DE90 008329

TENSILE FRACTURE TOUGHNESS OF CERAMIC MATERIALS: EFFECTS OF DYNAMIC LOADING AND ELEVATED TEMPERATURES

S. Suresh, T. Nakamura*, Y. Yeshurun†, K. Yang‡ and J. Duffy

Division of Engineering
Brown University
Providence, Rhode Island 02912, U.S.A.

*Department of Mechanical Engineering
State University of New York
Stony Brook, New York 11794, U.S.A.

†Present address: RAFAEL, Armament Development Authority
31021 Haifa, Israel

‡Present address: The Dow Chemical Co., Advanced Ceramics Laboratory
Midland, Michigan 48674, U.S.A.

DISCLAIMER

This report was prepared as an account of work sponsored by an agency of the United States Government. Neither the United States Government nor any agency thereof, nor any of their employees, makes any warranty, express or implied, or assumes any legal liability or responsibility for the accuracy, completeness, or usefulness of any information, apparatus, product, or process disclosed, or represents that its use would not infringe privately owned rights. Reference herein to any specific commercial product, process, or service by trade name, trademark, manufacturer, or otherwise does not necessarily constitute or imply its endorsement, recommendation, or favoring by the United States Government or any agency thereof. The views and opinions of authors expressed herein do not necessarily state or reflect those of the United States Government or any agency thereof.

MASTER

DISTRIBUTION OF THIS DOCUMENT IS UNLIMITED

DISCLAIMER

This report was prepared as an account of work sponsored by an agency of the United States Government. Neither the United States Government nor any agency thereof, nor any of their employees, makes any warranty, express or implied, or assumes any legal liability or responsibility for the accuracy, completeness, or usefulness of any information, apparatus, product, or process disclosed, or represents that its use would not infringe privately owned rights. Reference herein to any specific commercial product, process, or service by trade name, trademark, manufacturer, or otherwise does not necessarily constitute or imply its endorsement, recommendation, or favoring by the United States Government or any agency thereof. The views and opinions of authors expressed herein do not necessarily state or reflect those of the United States Government or any agency thereof.

DISCLAIMER

Portions of this document may be illegible in electronic image products. Images are produced from the best available original document.

TENSILE FRACTURE TOUGHNESS OF CERAMIC MATERIALS: EFFECTS OF DYNAMIC LOADING AND ELEVATED TEMPERATURES

S. Suresh, T. Nakamura, Y. Yeshurun, K. Yang and J. Duffy

Abstract

Experimental methods are presented for the determination of fracture inititiation toughness of ceramics and ceramic composites in pure tension under quasi-static and dynamic loading conditions over a range of temperature spanning 20°C to 1300°C. Circumferentially notched and cyclic fatigue pre-cracked rods of a variety of ceramic materials were subjected to quasi-static tensile fracture (stress intensity factor loading rate, $\dot{K}_I \approx 0.1\text{MPa}\sqrt{\text{m}} \cdot s^{-1}$) in an electro-servohydraulic test machine and to dynamic tensile fracture ($\dot{K}_I \approx 10^6\text{MPa}\sqrt{\text{m}} \cdot s^{-1}$) using a modified tensile Kolsky (split-Hopkinson) bar. For the quasi-static and dynamic fracture tests at elevated temperatures, the ceramic specimen was inserted in an air furnace where either friction grips or stress wave loading outside the furnace subjected the specimen to fracture. Dynamic finite element analyses of the circumferentially notched cylindrical rod have been conducted to develop the optimum specimen dimensions and test procedures for ambient and elevated temperature dynamic fracture initiation toughness measurement.

Experiments conducted on Al_2O_3, Si_3N_4 and SiC, and an Al_2O_3–25 volume% SiC whisker composite at room temperature indicate that the dynamic to quasi-static fracture initiation toughness ratio K_{Id}/K_{Ic} is in the range of 1.1–1.4. Elevated temperature fracture tests for the polycrystalline Al_2O_3 of $3\mu m$ average grain size reveal that K_{Id} is only mildly sensitive to temperature over a range of 20°C–1100°C, whereas it suffers a precipitous drop above 1100°C. Over the temperature range 20°C–1300°C, the ratio K_{Id}/K_{Ic} is found to be in the range 1.2–1.5. Scanning electron microscopy observations show that failure above 1100°C usually evolves by the nucleation, growth and coalescence of cavities. The mechanisms of elevated temperature quasi-static and dynamic fracture in polycrystalline Al_2O_3 are examined and possible causes for the apparently higher dynamic fracture initiation resistance are discussed. The significance and limitations of the proposed experimental techniques are highlighted.

I. INTRODUCTION

Increasing technological interest in the development of high performance propulsion systems has led to a surge in research activity focussing on a wide variety of elevated temperature materials. Ceramics and ceramic-matrix composites are candidate materials for potential structural components in such high performance engine applications. The mechanisms of quasi-static fracture in ceramics at ambient temperature have been the subject of much research in the recent past. However, in service, ceramic components may be subjected, whether by design or otherwise, to dynamic loading conditions. It is, therefore, essential to gain a detailed understanding of their dynamic fracture initiation characteristics. Additionally, there is a paucity of information on the fracture properties of ceramics at elevated temperatures which are representative of potential service conditions. This lack of a reliable data base is principally due to the experimental problems in conducting elevated temperature fracture tests, especially in a pure tensile loading mode.

Because of its low cost and ease of testing, the Charpy impact test has been the most widely used dynamic fracture experiment. The standard Charpy test provides only the impact resistance in terms of the total absorbed energy, which is comprised of contributions from both crack initiation and crack growth processes. Consequently, nonconservative estimates of critical fracture parameters may result from such an experiment. Although the Charpy test is often useful for screening purposes in the materials selection process, the interpretation of results in terms of fracture mechanics concepts is not unambiguous [1]. Therefore, the instrumented Charpy test has been used to determine the dynamic fracture characteristics of ceramics in conjunction with the fracture mechanics approach. The static fracture analysis for obtaining dynamic fracture initiation toughness, K_{Id}, values from instrumented Charpy impact testing requires the determination of the maximum fracture load in the load-time record. The resulting analysis thus reduces the instrumented Charpy test to a quasi-static condition which, in part, defeats the original purpose of the test. Plane strain conditions are also not achieved uniformly along the crack front in the Charpy test. Recent analyses have shown that smooth monotonic loading conditions may not prevail in the crack-tip region in a dynamic Charpy (three-point bend bar) test specimen [3].

Recently Duffy, Suresh and coworkers [3-5] presented experimental techniques for the determination of dynamic fracture initiation toughness at room temperature under conditions of pure mode I or mode III loading using a modified tensile Kolsky (split-Hopkinson) bar. These earlier studies focussed primarily on the dynamic fracture toughness measure-

ment of an alumina ceramic and hence specific test methods were developed for avoiding impedance mismatch between the steel loading bars and alumina.

In this paper, we discuss experimental methods for the determination of the effects of loading rate and test temperature on the fracture initiation toughness in a wide variety of ceramic materials. The present work involves the development of the following novel experimental procedures and analyses for the dynamic fracture toughness determination in brittle materials: (i) The design of specimen geometry and optimization of strain gage locations for critical load measurements under dynamic fracture conditions, as guided by a detailed finite element analysis of the stress field in the dynamic test set-up. (ii) Experimental measurement of the dynamic and quasi-static fracture initiation toughness in cyclic fatigue pre-cracked ceramic rods whereby an unambiguous determination of the stress intensity factor values can be obtained with the use of conventional fracture mechanics (similar to the techniques commonly employed for ductile metallic materials). (iii) The determination of quasi-static fracture toughness in pure tension over a range of temperatures spanning 20°C–1300°C, using the same specimen geometry as that employed in the dynamic fracture tests. (iv) Development of test methods, guided by finite element analyses, for the determination of dynamic tensile fracture toughness at elevated temperatures. The mechanisms underlying the effects of loading rate and test temperature on fracture initiation toughness are discussed. The implications of the experimental results are also examined in the context of currently available analytical models for the dynamic fracture resistance of ceramic materials.

II. MATERIALS AND EXPERIMENTAL METHODS

Quasi-static and dynamic tensile fracture experiments were conducted at room temperature on a variety of ceramic materials which included Al_2O_3, Si_3N_4, and SiC, as well as an Al_2O_3–25 volume% SiC whisker composite. Details of the microstructures and room temperature mechanical properties of these materials are listed in Table I. Elevated temperature fracture tests under both quasi-static and dynamic loading conditions were conducted on the AD 998 alumina ceramic at 900°C, 1100°C and 1300°C.

(1) Room Temperature Fracture Experiments

The geometry of the test specimen used for the dynamic fracture experiments is schematically shown in Figure 1. The circumferentially notched cylindrical specimens

of all the ceramic materials had the following dimensions: d_i = 9 mm, L = 33.6 mm, L_1 = 25.4 mm, t = 1.8 mm, θ = 60°, and ρ = 0.125 mm. The outer diameter, d_o, was 19 mm for Al_2O_3 and Al_2O_3–SiC composite, 15.9 mm for SiC and 15.24 mm for Si_3N_4. These variations in the outer diameter of the specimen were a consequence of the need for procuring the different ceramic materials studied in this work from different commercial sources.*

In order to obtain a measure of the quasi-static and dynamic fracture initiation toughness values that are independent of the notch-tip geometry, it is essential to introduce a sharp fatigue pre-crack at the notch-tip prior to the fracture toughness test. The specimens were fatigue pre-cracked under fully compressive cyclic loads using the procedure developed by Suresh and coworkers [6-8]. In this method, the test specimens were subjected to uniaxial cyclic compression in an electro-servohydraulic machine over a stress range of –50 MPa to –785 MPa at a constant frequency of 15Hz (sinusoidal waveform) in the laboratory environment (temperature ≈ 20°C and relative humidity ≈ 40%). For the notch geometry (Figure 1) and loading conditions, a self-arresting mode I fatigue crack propagated along the plane of the notch over a distance of 70–200μm depending on the test material. (See refs. [6-8] for details of the mechanisms of fatigue crack growth in cyclic compression). The presence of a concentric and uniform crack front ahead of the notch-tip was ensured *a posteriori* through optical and scanning electron microscopy observations after the completion of the fracture test. For the brittle ceramic materials, the plane strain fracture toughness, K_{Ic}, values for the circumferentially notched cylindrical rod specimens used in this study are obtained from the expression (e.g., [9])

$$K_I = \frac{P}{\pi R^2}\sqrt{\pi R}\; F(2R/D) \tag{2.1}$$

where R is the radius of the remaining circular ligament (= $d_i/2$ minus the depth of the fatigue pre-crack), P is the applied load, D is the outer diameter of the bar, and $F(2R/D)$ is a size function which is tabulated in all the standard handbooks of stress intensity factors (e.g., [9]). The load P used in calculating K_{Id} with Eq. (2.1) is equal to the maximum load transmitted through the ligament during passage of the stress pulse.

* It should be noted that the uncracked ligament diameter (prior to the commencement of the dynamic fracture test), as well as the diameter of the steel loading bars and the locations of the strain gages for monitoring the transmitted pulse (to be discussed in detail later in this section) were approximately the same for all the ceramic materials.

In order to use the above formula for the calculation of plane strain fracture toughness, it is necessary to ensure that the fatigue crack is deep enough to be free of the strain field of the notch-root during the fracture experiment. The *minimum* length of the fatigue crack necessary to avoid the strain field effects of the notch-tip (when using the above standard expression for K_I) can be estimated in the following manner. Consider a very large elastic plate containing a circular hole of radius c at its center. Let a mode I crack of length l emanate from the hole. It is a well known result from both analytical models and finite element calculations (see, for example, refs. [10-12]) that the transition crack size, l_o, beyond which the standard expressions for K_I (such as Eq. (2.1)) derived for long flaws are unambiguously valid, is

$$l_o = c/[(1.12k_t/\bar{F})^2 + 1] \tag{2.2}$$

where k_t is the elastic stress concentration factor (equal to 3 for a circular hole under far-field axial stress), $\bar{F}$ is a dimensionless function of geometry (of order unity) which is the correction factor to allow for the finite width of the plate, and the multiplier 1.12 is the free surface correction factor. For a fatigue crack emanating from a central hole in the brittle plate, $l_o \approx 0.1R$. For single edge-notched brittle plates and circumferentially notched brittle rods, values of l_o are generally a small fraction of the notch-root radius ρ; for moderate to sharp notches in brittle solids (as in the present experiments), they generally fall in the range $\rho/20$ to $\rho/4$. Thus, it is seen that, for the present set of experiments on circumferentially notched polycrystalline ceramics, the compression fatigue pre-crack is significantly longer than the critical size required to avoid the artifacts of notch geometry. Furthermore, it is important to note that the size of the fatigue pre-crack is substantially greater than the characteristic microstructural dimension (e.g., grain size) for all the materials investigated in this study.

The room temperature dynamic fracture initiation tests were conducted using the experimental arrangement schematically illustrated in Figure 2. Stress wave loading of the notched and fatigue pre-cracked bar in tension is accomplished by recourse to the method developed by Costin et al [13] for metals. The ceramic specimen is held between two long steel bars each of which is 25.4 mm in diameter. For secure gripping, the specimen is inserted within two axial holes machined into the ends of the steel bars and held in place by a cemented joint. Precise machining and a fine air vent are used to avoid any gap between the ends of the ceramic specimen and the steel bars. The detonation of a controlled amount

of explosive against a specially designed loading head at the end of the bar generates a tensile pulse which propagates down the bar and subjects the pre-cracked cross section of the ceramic to dynamic fracture. Part of this pulse is transmitted through the fractured ceramic ligament into the steel transmitter bar and is measured by strain gages located as shown in Figure 2. The elapsed time between the arrival of the pulse at the pre-cracked cross section and the onset of catastrophic fracture is approximately 10–20 μsecs. This corresponds to a stress intensity factor rate, $\dot{K}_I \approx 10^6$ MPa$\sqrt{\text{m}} \cdot s^{-1}$. This loading rate is some three orders of magnitude higher than that achievable in an electro-servohydraulic test machine. Detailed finite element analyses, discussed in the next section, indicate that the proximity of the transmitter strain gages to the ends of the ceramic specimen as well as the length of the ceramic specimen can affect the measurement of the load at the fracturing ligament. Numerical calculations, however, also reveal that if the specimen length on the transmitting side is about 1/3 of its outer diameter, a "cleaner" pulse is transmitted to the steel bar.

Precise determination of the dynamic fracture initiation toughness requires the ability to measure the pulse transmitted through the uncracked ligament. This is achieved by using strain gages placed on the outer surface of the steel bar at the downstream side of the crack plane. However, a detailed finite element calculation is required to interpret correctly the output of the gages on the steel bar in terms of load at the fracture site. In the room temperature experiments, the testing geometry is composed of the steel loading bars and the ceramic specimen. In one-dimensional models, the extent of wave transmission and reflection at the interface can be given by the mismatch of impedance in the two materials. However, in the current model, states of wave propagation are extremely complex near the ceramic-steel boundary due to its shape and proximity to the crack, and the wave patterns cannot be determined simply from the impedance mismatch. Therefore, we have carried out finite element simulations with the specific purpose of determining the difference in the load transmitted between the ligament and the downstream gage location (see Figure 2). As described in detail in Section 3, the computational results confirm that such differences are less than 2% for all the combinations of steel loading bar and ceramic materials tested in this investigation.

The choice of a suitable location for mounting the strain gages is dictated by two competing criteria. From the viewpoint of preserving the pulse shape or of minimizing the amount of attenuation, the distance between the crack and the gage should be small. How-

ever, the gage must also be sufficiently far away from the crack plane and the ceramic-steel boundary so that the axial stress is uniform across the section. In the room temperature tests, the optimum gage location is determined from the finite element analyses to be 25 mm downstream from the crack. This distance equals the outer diameter of the steel rod.

Quasi-static fracture initiation tests ($\dot{K}_I \approx 0.1$ MPa$\sqrt{\text{m}} \cdot s^{-1}$) were carried out using specimen geometry, notch geometry and pre-cracking procedure which were the same as in the dynamic tests, with the only exception that the length dimension of the ceramic rods was L = 115 mm. The loading rate in the electro-servohydraulic machines was about 25 mm/min. for all the fracture tests. Further details on the procedures for the room temperature tensile fracture toughness measurements under quasi-static loading conditions can be found in ref. [8].

(2) Elevated Temperature Fracture Toughness Measurements

Elevated temperature dynamic fracture initiation tests were carried out on the AD 998 alumina ceramic at temperatures of 900°C, 1100°C, and 1300°C. For this purpose, a much longer specimen ($L = 45.8cm$) than the one used for the room temperature tests was designed, but the rod diameter and dimensions of the notch were identical to those used in the room temperature experiments. The notch was located midway along the length of the specimen. The ceramic specimen was fatigue-precracked under far-field cyclic compression using the procedure described earlier in Section 2.1. For the present case, however, special precautions were taken to avoid misalignment of the long rod; the specimen was placed between a fixed flat surface and a parallel surface housed on a grease-lubricated hemi-spherical seat in the servohydraulic test machine. For the specimen and loading conditions employed, there was no buckling of the specimen and a concentric fatigue crack was observed around the root of the notch.

The precracked ceramic rod was inserted into an ATS air furnace* where the plane of the notch was located at the center of the heat zone (Figure 3). The furnace has a temperature capability of ±1°C over the range of 900–1300°C. The heating or cooling rates to or from the test temperature were kept below 15°C/min. to avoid possible thermal shock effects. The ends of the ceramic rod extended outside the furnace to make it possible to grip the ceramic rod through cemented joints. For the dynamic fracture tests, the loading end of the specimen was cemented to the steel bar through which the incident tensile pulse

* Applied Test Systems, Butler, PA

was transmitted. The other end of the specimen was cemented to a cylindrical rod of the same alumina ceramic for the purpose of sufficiently delaying the return of the pulse reflected from the farther end of the bar so that it did not overlap or interfere with the record of the transmitted pulse. Since a strain gage must be placed outside the furnace, it was located on the ceramic rod at a distance of 207 mm from the crack plane (see Section 3). Since the pulse was propagated along the entire length of the specimen in the elevated temperature tests, it encountered gradients in mechanical properties along the length of the specimen as a consequence of temperature gradients. Figure 4 shows a typical temperature profile along the specimen (measured by means of thermocouples) for the dynamic fracture specimen heated to a temperature of 1300°C in the air furnace.*

High temperature quasi-static fracture tests were conducted on notched and compression fatigue pre-cracked alumina rods having the same dimensions as those used in the dynamic fracture experiments. After pre-cracking, the specimen was inserted into the ATS air furnace located in an Instron electro-servohydraulic machine. The ends of the specimen, located outside the furnace were friction-gripped with the same arrangement used for the room temperature tests (see Section 2.1). A schematic diagram of the high temperature quasi-static fracture test arrangement is shown in Figure 5.

III. FINITE ELEMENT CALCULATIONS

A detailed finite element analysis of the stress field in the interior of the dynamic fracture specimen and its interfaces with the loading bars has been conducted with the dual objective of (i) optimizing the specimen geometry and strain gage locations for the unambiguous interpretation of dynamic fracture initiation toughness and (ii) checking the validity of the dynamic fracture toughness measurements. The computational analysis was carried out for each ceramic material examined in this study at room temperature and for Al_2O_3 at elevated temperatures using the finite element code ABAQUS [14].

* In an attempt to check that the measured value of the dynamic fracture initiation toughness is not influenced by the specimen geometry, experiments were conducted at 20°C using the long, elevated temperature test specimen without heating the furnace. It was found that the K_{Id} values determined from the specimen geometry and test arrangement shown in Figure 3 were essentially the same as those measured with the shorter specimen arrangement of Figures 1 and 2. This result provides a confirmation of the validity of the present experimental test procedure.

(1) Analysis of Room Temperature Tests

The finite element model for the room temperature tests consisted of 798 eight-noded elements, Figure 6. An elastic material model was used within the context of an axisymmetric formulation. The region analyzed extends over 100 mm ($\sim 4D$, where D is the outer diameter of the steel bar) on either side of the crack plane and thus includes the entire ceramic specimen, the joints with the steel bar and a portion of the steel bar both upstream and downstream. During the time interval of interest, the unloading waves generated from the ends of the bar reach neither the crack region nor the strain gage location. The near-crack region of the mesh which contains the complete ceramic specimen and parts of the steel bar/casing is shown in Figure 6. (However, the analysis, covering a distance of 100 mm, extends beyond the region shown). The ceramic specimen (region contained within the heavy lines) has a diameter of $d_o = 0.75D$ for Al_2O_3 and extends a distance of D upstream (direction of incoming tensile pulse) and a distance of $0.25D$ downstream. The undeformed notch-tip geometry has an initial opening of $0.07D$. The actual crack-tip is located just inside the notch-root where it has zero opening dimension (representative of a fatigue crack). The diameter of the uncracked ligament is $0.35D$. The transmitter strain gage is located at a distance of approximately D downstream from the crack, as indicated in Figure 6. The model assumes that both materials remain elastic during passage of the pulse. Material properties for the steel were chosen to be: Young's modulus, $E_s = 200GPa$, Poisson's ratio, $\nu_s = 0.3$, and mass density, $\rho_s = 7800$ kg/m^3. The material properties used in the computations for the ceramic materials are as listed in Table I.

A tensile load (P_{app}) was applied at the upstream end of the bar, and the finite element computation was carried out for at least 30 $\mu sec.$ beyond the instant when the pulse has passed through the strain gage location. The time history of the applied load is chosen so that the pulse shape at the gage location is similar to the one measured in the experiment.

The computed loads through the uncracked ligament and the gage location for Al_2O_3 and SiC at room temperature are plotted as functions of the elapsed time in Figures 7(A) and 7(B), respectively. The time is measured after the arrival of the initial loading pulse at the crack and the ligament load is the exact net force across the uncracked ligament plane. The transmitted pulse at the gage location (25 mm downstream) is obtained by multiplying the axial stress near the surface with the cross-sectional area of the bar. This pulse closely approximates the actual pulse measured by the strain gages in the dynamic fracture experiments. The instantaneous values of both the ligament load and the transmitted pulse

are normalized by the maximum load attained by the ligament, P_{lig}^{max}. Figures 7(A) and (B) show that there is a nearly constant time lag of about 4 $\mu sec.$ between the ligament load for both Al_2O_3 and SiC, and the transmitted pulse, and that the maximum value of the transmitted pulse is equal to about P_{lig}^{max}. This result indicates that there is only a very small amount of wave reflection at the ceramic-steel boundaries near the crack. At the downstream gage location, the computed state of stress is found to be nearly uniform across the section of the bar, thereby suggesting that any wave dispersion created by the near-crack geometry vanishes at a distance of $\sim D$ downstream. These computational results validate the suitability of the strain gage location as well as the correctness of the specimen geometry. For the other ceramic materials, the results of the finite element computations are qualitatively identical to those discussed here for the Al_2O_3 and SiC. The only difference that arises for the different materials is the time lag between the incident and transmitted pulses.

The dynamic stress intensity factor based on Eq. (2.1) is computed with the load based on the transmitted pulse. In addition, we have calculated the precise dynamic stress intensity factor using the axisymmetric J-integral under dynamic condition (see, for example, Nakamura et al [15]). This J-integral is determined by integrating the field quantitites over a domain whereby the most accurate determination of the stress intensity factor is accomplished in the finite element procedure. The computed K_I and that determined from the measured load are almost identical functions of time with a constant time lag. This lends further support to our capability to measure accurately the dynamic K_I from the record of the transmitter strain gage.

(2) Analysis of Elevated Temperature Tests

A similar but much longer specimen model (length = 510 mm, 1232 elements) was employed in the finite element simulations for the elevated temperature tests. In the calculations, the larger length of bar was necessitated by the greater distance between the crack plane and the strain gage location. Additionally, the elevated temperature computational model was applied only to the ceramic (Al_2O_3), since all measurements were made directly on the ceramic surface (Figure 3). In order to take the temperature gradient along the ceramic bars into account, it was necessary to make separate experimental measurements of temperature profiles along the ceramic bar on either side of the notch (e.g., Figure 4). This enables us to incorporate into the numerical model the variation of Young's modulus with

temperature along the bar. Values of the Young's modulus at elevated temperature were taken from the work of Springgs et al [16] who used three-point bend testing to measure the Young's modulus of Al_2O_3 over a wide range of temperatures. Based on this earlier study and from the references cited therein, the Young's modulus values were taken to be 345, 345, 254, and 162 GPa at 20, 900, 1100, and 1300°C, respectively. Variations of mass density and Poisson's ratio with temperature and rate-dependent effects were neglected.

As in the room temperature simulations, a tensile load was applied at the upstream end of the bar. The transmitted pulse at the gage location (207 mm downstream) was obtained by multiplying the axial stress at the element closest to the free surface by the cross-sectional area of the bar. The normalized values of the ligament load and transmitted pulse for the Al_2O_3 at temperatures of 900°C, 1100°C and 1300°C are shown in Figures 8(A), (B), and (C), respectively. Although not shown here, the results of room temperature calculations for the same geometry of Al_2O_3 indicated that the peak transmitted pulse was 2% smaller than the maximum ligament load (due to wave attenuation between the two locations). In the elevated temperature tests, the thermal gradient causes the wave speed and the peak level of the pulse to vary along the length of ceramic rod. Since the Young's modulus at the high temperature ligament region is smaller than the room temperature gage location downstream, the peak level of the load at the gage location tends to rise. At 900°C, this effect offsets the geometrical attenuation, and the two peak pulse values are nearly identical. At higher temperatures, the peak transmitted pulse increases as the variation in Young's modulus along the rod increases. The discrepancy between the values of the peak ligament load and the maximum transmitted load at the gage location is 6% at 1100°C and 18% at 1300°C.* A varying wave speed also affects the time lag between the pulses at different temperatures. The change in wave speed with temperature was inferred from the temperature dependence of Young's modulus for Al_2O_3.

Whereas only the geometric dispersion of the propagating pulse needs to be accounted for in the room temperature dynamic tests, it is important to note that there are more possible sources of error in the high temperature experiments. Firstly, the temperature gradient along the length of the ceramic rod needs to be measured precisely. In addition, the dependence of wave velocity on temperature for the particular material must be known.

* These computed differences between the peak values of the ligament load and transmitted load have been used to recalibrate the experimental measurements made at the strain gage locations (see Table III and Figure 12).

Accurate measurements of both the temperature gradient and the values of wave velocity as a function of temperature require independent tests.

IV. RESULTS

(1) Room Temperature Fracture Tests

The quasi-static and dynamic fracture initiation toughness values at room temperature for all the ceramic materials investigated in this work are summarized in Table II. It is found that for all the monolithic ceramics and the Al_2O_3-SiC composite, the K_{Id}/K_{Ic} ratio falls within the range of 1.1–1.4. While Al_2O_3 and SiC exhibit a dynamic to static fracture toughness ratio of 1.28 and 1.1, respectively, Si_3N_4 has a dynamic toughness value which is about 40% higher than the corresponding quasi-static value. Also listed in Table II are the experimental results reported by Yang et al [17] for Al_2O_3 and Al_2O_3–25 vol.% SiC whisker composite based on quasi-static and Charpy impact tests on a three-point bend bar. It is interesting to note that for alumina, the present experimental ratio, K_{Id}/K_{Ic}, obtained using the modified tensile Kolsky bar, is comparable to the toughness ratio of 1.33 reported by Yang et al [17] based on a drop-weight impact test. The values reported in Table II from the present work represent an average of at least two measurements for all the ceramics. For the case of alumina, at least four tests were conducted in each of the quasi-static and dynamic conditions. The typical variation in the toughness values observed for the fine-grained alumina was $\pm 0.2 \mathrm{MPa}\sqrt{\mathrm{m}}$ for both the strain rates.

Figures 9(A) and 9(B) show examples of the macroscopic appearance of the mode I dynamic fracture surfaces of Al_2O_3 and SiC, respectively. Similar macro-modes of failure were also observed in Si_3N_4 and Al_2O_3–SiC whisker composite. The purely tensile nature of the loading is evident from the flat fracture surfaces observed in these cases. Figures 10(A) and 10(B) show examples of the fatigue pre-crack, about 110 and 80 μm in depth, at the root of the circumferential notch in the Al_2O_3 and SiC specimens, respectively, which were subjected to dynamic fracture.

In the interest of brevity and in view of subsequent discussions on high temperature fracture toughness, we confine our attention here only to a description of the microscopic failure modes observed in the alumina ceramic. Figures 11(A) and 11(B) show scanning electron fractographs of the dynamic fracture initiation region for the alumina at two different magnifications. Here, predominantly intergranular fracture with evidence of sporadic transgranular cleavage was observed. This mode of failure is similar to that reported ear-

lier by Suresh and Tschegg [8] for the quasi-static fracture of the same mateial. Although small differences in the extent of intergranular fracture were noticed between the static and dynamic tests, they did not appear to be statistically significant. A predominantly intergranular mode of failure was also observed for all the other ceramic materials.

(2) Elevated Temperature Fracture Tests

Figure 12 and Table III illustrate the influence of test temperature on the quasi-static and dynamic fracture initiation toughness values measured for the Al_2O_3 ceramic. Over the entire range of temperatures investigated, the dynamic fracture toughness was higher than the quasi-static value. Both K_{Id} and K_{Ic} values decreased precipitously with an increase in temperature beyond 1100°C, although the toughness values declined only moderately with temperature below 1100°C. Note that the K_{Id} values, shown in Table III and Figure 12, account for the differences between the ligament load and the transmitted pulse at elevated temperatures (shown in Figure 8).

The principal reason for the deterioration in fracture initiation resistance with increases in temperature was identified to be cracking along the grain boundaries. The propensity for grain boundary separation increased dramatically above a temperature of 1100°C. Figure 13 shows an example of a cross section of the specimen where cracking along grain boundaries is clearly evident beneath the fracture surface.* The effects of such intergranular microfracture on creep deformation and fracture in ceramic materials have been the subject of detailed investigations in recent years (e.g., [18-22]).

V. DISCUSSION

There have been prior attempts to determine the strain rate dependence of compressive strength in ceramics using the compression (split-Hopkinson) bar (e.g., [23]). However, there have been no attempts to date to determine dynamic tensile fracture toughness of ceramics as a function of temperature. Experimental procedures have been developed in

* Recent studies by Han and Suresh [18] have shown that, in SiC whisker-reinforced Al_2O_3, the oxidation of SiC in high temperature air environment leads to the formation of an amorphous glass phase. The viscous flow of the glass causes extensive cavitation along the matrix grain boundaries and the interfaces between the matrix and the reinforcement. Thus the effects of intergranular cracking on high temperature K_{Id} and K_{Ic} values seen for Al_2O_3 will be expected to be even more pronounced for the case of Al_2O_3–SiC composites.

this work which offer new possibilities for the determination of fracture initiation toughness in ceramics and discontinuously reinforced ceramic composites over a wide range of temperatures and loading rates. Experimental results obtained for a variety of monolithic ceramics and a ceramic composite demonstrate the capability of the proposed methods to yield reliable and reproducible measurements of critical fracture parameters. The test methods employed in this study include several new developments: (i) The techniques provide a means for conducting a fracture toughness test in a simple specimen geometry which can be tested quasi-statically (in an electro-servohydraulic machine) and dynamically (in a tensile Kolsky bar arrangement) with the same cross-sectional geometry and pre-cracking method. (Only changes in the length of the specimen are necessary for testing at different loading rates and temperature regimes). (ii) It has been demonstrated that stable Mode I fatigue pre-cracks can be introduced in the circumferentially notched ceramic rods by recourse to precracking in cyclic compression. This provides an unambiguous interpretation of fracture toughness based on standard stress intensity factor calibrations for notched rods (e.g., [9]). The cyclic compression method employed in this study is the only known technique whereby concentric fatigue cracks can be introduced in cylindrical rods of brittle solids at room temperature.* (iii) The test methods employ a combined experimental and numerical calibration whereby fracture initiation toughness values can be determined to a good degree of accuracy even when the ceramic test specimens have an impedance mismatch with respect to the steel loading bars. (iv) Both the quasi-static and dynamic fracture tests at ambient and elevated temperature can be conducted in a purely *tensile* loading mode where the state of stress at the fracture site is unambiguous. (v) The stress intensity factor rate, $\dot{K}_I$, that can be realized in the Kolsky bar arrangement is significantly greater than that obtainable in a Charpy impact test.

There are, however, certain limitations associated with the experimental techniques employed in this work. (i) The determination of optimum experimental conditions (e.g., the choice of strain gage locations for the dynamic fracture tests) and the interpretation of experimental results for both the ambient and elevated temperature tests require detailed finite element calculations to be conducted in conjunction with the experiments for each material, specimen geometry and test temperature. (ii) The experimental method requires

* Fracture tests conducted on notched ceramic materials without sharp fatigue cracks can lead to anomalously high values of K_{Id} and K_{Ic}, with the measured toughness value being highly sensitive to the acuity of the notch-tip (see, for example, ref. [5]).

specialized facilities and strict safety procedures; however, the tests can be conducted routinely once the experimental set-up is operational. (iii) The procedure allows for direct tensile fracture testing of ceramics at elevated temperatures, but requires a very long test specimen. (iv) For the elevated temperature fracture tests, there are some uncertainties in the variation of elastic properties with temperature gradients in the specimen. Therefore, the errors in the finite element analyses are likely to be greater for the higher temperature experiments. This last limitation is probably applicable to other test methods as well.

It is instructive to examine the present experimental results in the context of currently available theories of dynamic fracture in ceramic materials. Recently, Brockenbrough, Suresh and Duffy [24] conducted an analysis of dynamic fracture in microcracking brittle solids where the ratio of dynamic to static fracture toughness was explicitly determined as a function of microcrack velocity and elastic properties. A model was proposed to determine the stiffness loss caused by a dilute population of microcracks aligned in a direction normal to the far-field tensile stress axis. The model invoked the criterion that microcrack coalescence and macrocrack initiation occurred in the static and dynamic loading situations when the average opening displacement of the microcracks (which is a function of the loading rate) reached a critical value. Figure 14 shows the predicted variation of the K_{Id}/K_{Ic} ratio as a function Poisson's ratio and microcrack velocity, V (normalized by the Rayleigh wave speed, C_R), from ref. [24]. Based on the above model, it is seen that when microcracking is the dominant mode of crack-tip damage, the dynamic to static fracture initiation toughness values are expected to lie within the range 1.0–1.75. Also shown in this figure are the experimentally determined K_{Id}/K_{Ic} ratios from the present study for all the room temperature and elevated temperature fracture tests. All the experimental results obtained in this study are found to lie within the bounds predicted by the analysis. It is also interesting to note that the room temperature dynamic fracture data of Yang et al [17] obtained using the instrumented Charpy tests on polycrystalline alumina and on Al_2O_3–25 vol.% SiC whisker composite show (see Table II) a K_{Id}/K_{Ic} ratio of 1.33 and 1.2, respectively, which also fall within the range of values expected from the microcracking model.

There are several aspects of the dynamic fracture tests which warrant detailed further investigations: (i) Although there is clear evidence of grain boundary microcracking in the elevated temperature quasi-static and dynamic fracture test specimens, direct observations of crack-tip microcracking at room temperature have yet to be obtained. It is noted,

however, that high magnification fractographs, such as Figures 11a and 11b which show failure along grain facets, provide some indirect evidence of the possibility of intergranular microfracture. It is also known that precracking in cyclic compression promotes grain boundary microcracking ahead of the notch-tip [6]. Additionally, very high strain rate dynamic tests conducted on polycrystalline alumina using the plate impact experiments have documented the nucleation of microcracks upon the passage of the stress pulse [25]. (ii) Existing analyses of dynamic fracture in ceramics, such as those presented in [24], invoke the assumption of anisotropic microfracture where the internal flaws are assumed aligned normal to the far-field loading direction. More realistic descriptions warrant analyses of random orientations of microcracks for the polycrystalline ceramic with an equiaxed grain structure. (These analyses, however, will introduce additional complications associated with the mixed-mode opening of microdefects). (iii) Refinements to the present finite element analysis for the high temperature dynamic fracture tests for alumina will inevitably require a detailed experimental investigation of the changes in elastic properties with temperature. (iv) The present work has documented novel experimental methods for the fracture testing of a wide range of monolithic and discontinuously-reinforced ceramics under dynamic loads and elevated temperatures. In addition, a general theoretical framework for the apparently higher fracture toughness at faster loading rates has been presented in conjunction with our earlier work [24]. However, more detailed microscopic analysis of the failure processes in each ceramic material (investigated in this work) is necessary to pinpoint the origin of the differences in the K_{Id}/K_{Ic} ratios among the different materials.

VI. CONCLUSIONS

1. New experimental methods are proposed for the determination of purely tensile fracture initiation toughness in ceramics and discontinuously-reinforced ceramic composites over a temperature range of 20°C to 1300°C at dynamic stress intensity factor rates, $\dot{K}_I \approx 10^6 \mathrm{MPa}\sqrt{\mathrm{m}} \cdot s^{-1}$ using a modified tensile Kolsky bar. The specimen geometry employed is a circumferentially-notched and cyclic fatigue pre-cracked rod. Dynamic finite element analyses have been conducted to develop optimum specimen dimensions and test procedures for ambient and elevated temperature dynamic fracture initiation toughness measurement. The methods proposed here offer new possibilities for the determination of tensile fracture initiation toughness in ceramic materials as a function of temperature and

loading rate.

2. With the proposed experimental techniques, quasi-static fracture toughness can be measured at both ambient and elevated temperatures using a similar specimen geometry and precracking method for comparisons with the dynamic fracture toughness data.

3. Experiments conducted on a wide variety of monolithic ceramics, viz., polycrystalline Al_2O_3, Si_3N_4 and SiC, and an Al_2O_3-25 vol.% SiC whisker composite at room temperature reveal that the dynamic to static fracture toughness ratio is in the range of 1.1–1.4.

4. Over the entire range of temperatures investigated, the dynamic fracture toughness of Al_2O_3 was higher than the quasi-static value. Values of K_{Id} decreased precipitously with an increase in temperature beyond 1100°C, although they exhibited only a modest drop with increasing temperature below 1100°C.

5. Grainboundary microcracking is found to be the principal cause of damage at elevated temperatures in both the quasi-static and dynamic fracture tests.

6. The experimentally determined dynamic to static fracture toughness ratio for all the ceramic materials investigated in this work falls within the bounds predicted by an analysis of dynamic fracture in microcracking media [24]. Although direct experimental evidence for microcracking was obtained in the high temperature fracture tests, further work is needed to identify the microscopic damage mechanisms at ambient temperature.

Acknowledgments— This work was supported partly by the Basic Sciences Division, U.S. Department of Energy under Grant DE-FG02-84ER-45167 to Brown University and partly by the Materials Research Group on Plasticity and Fracture in the Division of Engineering at Brown University which is funded by the National Science Foundation under Grant DMR-8714665. The finite element computations were made using the VAX Station 3500 at the State University of New York at Stony Brook. The authors are grateful to Mr. George LaBonte for his valuable help throughout the course of this work.

REFERENCES

[1] T. Kobayashi, M. Nilnomi, Y. Koide, and K. Matsunuma, "Instrumented Impact Testing of Ceramics"; in Proc. 2nd Conf. of Asia-Pacific Congress on Strength Evaluation. Seoul, Korea, 1989, in press.

[2] T. Nakamura, C.F. Shih, and L.B. Freund, "Three-Dimensional Transient Analysis of a Dynamically Loaded Three-Point Bend Ductile Fracture Specimen"; pp. 217-41 in Nonlinear Fracture Mechanics; Volume I – Time-Dependent Fracture, ASTM STP 995, Edited by A. Saxena, J.D. Landes, and J.L. Bassani, American Society for Testing and Materials, Philadelphia, PA, 1989.

[3] J. Duffy, S. Suresh, K. Cho and E. Bopp, "A Method for Dynamic Fracture Initiation Testing of Ceramics", *Journal of Engineering Materials and Technology, Trans. ASME*, **110**[4] 325-31 (1988).

[4] J. Duffy, S. Suresh, K. Cho and E. Bopp, "Addendum: A Method for Dynamic Fracture Initiation Testing of Ceramics", *Journal of Engineering Materials and Technology, Trans. ASME*, **111**[1] 86 (1989).

[5] J. Duffy, T. Nakamura, Y. Yeshurun and S. Suresh, "Dynamic Fracture of Ceramics"; pp. 355-62 in Mechanical Properties of Materials at High Rates of Strain, Conference Series No. 102, Edited by J. Harding, The Institue of Physics, IOP Publishing Ltd., Bristol, U.K., 1989.

[6] L. Ewart and S. Suresh, "Crack Propagation in Ceramics under Cyclic Loads", *Journal of Materials Science*, **22**[4] 1173-92 (1987).

[7] S. Suresh, L. Ewart, M. Maden, W. Slaughter and M. Nguyen, "Fracture Toughness Measurements in Ceramics: Precracking in Cyclic Compression", *Journal of Materials Science*, **22**[4] 1271-76 (1987).

[8] S. Suresh and E.K. Tschegg, "Combined Mode I–Mode III Fracture of Fatigue Precracked Alumina", *Journal of the American Ceramic Society*, **70**[10] 726-33 (1987).

[9] H. Tada, P.C. Paris and G.R. Irwin, The Stress Analysis of Cracks Handbook. Del Research Corporation, Hellertown, PA, 1985.

[10] N. E. Dowling, "Notched Member Fatigue Life Predictions Combining Crack Initiation and Propagation", *Fatigue of Engineering Materials Structures*, **2**[2] 129-38 (1979).

[11] J. C. Newman, Jr., "An Improved Method of Collocation for the Stress Analysis of Cracked Plates with Various Shaped Boundaries." NASA Technical Report No. TND-6376, National Aeronautics and Space Administration, Langley, Virginia (1971).

[12] S. Suresh, C.F. Shih, A. Morrone and N. O'Dowd, "Mixed-Mode Fracture Toughness of Ceramic Materials", *Journal of the American Ceramic Society*, in press.

[13] L.S. Costin, J. Duffy and L.B. Freund, "Fracture Initiation in Metals under Stress Wave Loading Conditions"; pp. 301-18 in Fast Fracture and Crack Arrest, ASTM STP **627**, Edited by G.T. Hahn and M.F. Kanninen, The American Society for Testing and Materials, Philadelphia, PA, 1976.

[14] ABAQUS, Version 4.3, Hibbitt, Karlsson and Sorensen, Inc., Providence, RI, 1989.

[15] T. Nakamura, C.F. Shih and L.B. Freund, "Elastic-Plastic Analysis of Dynamically Loaded Circumferentially Notched Round Bar", *Engineering Fracture Mechanics*, **22** [2] 437-52 (1985).

[16] R.M. Spriggs, J.B. Mitchell and T. Vasilos, "Mechanical Properties of Pure, Dense Aluminum Oxide as a Function of Temperature and Grain Size", *Journal of the American Ceramic Society*, **47** 323-27 (1964).

[17] K. Yang, A.S. Kobayashi and A.F. Emery, "Effects of LoadingRrate and Temperature on Dynamic Response of Ceramic Matrix Composites"; 3rd International Symposium on Ceramic Materials and Components for Engines, Las Vegas, Nov. 1988, in press.

[18] L.X. Han and S. Suresh, "High-Temperature Failure of an Alumina-Silicon Carbide Composite under Cyclic Loads: Mechanisms of Fatigue Crack-tip Damage", *Journal of the American Ceramic Society*, **72**[7] 1233-38 (1989).

[19] T.-J. Chuang and S.M. Wiederhorn, "Damage-Enhanced Creep in a Siliconized Silicon Carbide: Mechanics of Deformation", *Journal of the American Ceramic Society*, **71**[7] 595-601 (1988).

[20] G. Grathwohl, "Creep and Fracture of Hot-Pressed Silicon Nitride with Natural and Artificial Flaws", pp. 565-77 in Creep and Fracture of Engineering Materials and Structures, Edited by B. Wilshire and R. Owen, Pineridge, Swansea, U.K., 1984.

[21] A. Venkateswaran and D.P.H. Hasselman, "Role of Cracks in the Creep Deformation of Brittle Polycrystalline Ceramics", *Journal of Materials Science*, **18**[1] 161-72 (1983).

[22] S. Suresh and J.R. Brockenbrough, "A Theory for Creep by Interfacial Flaw Growth in Ceramics and Ceramic Composites", *Acta Metallurgica*, in press.

[23] J. Lankford, "Mechanisms Responsible for Strain-Rate Dependence of Compression Strength in Ceramics", *Journal of the American Ceramic Society*, **64**[1] C-33-34 (1981).

[24] J.R. Brockenbrough, S. Suresh and J. Duffy, "An Analysis of Dynamic Fracture in Microcracking Brittle Solids", *Philosophical Magazine A*, **58**[6] 619-34 (1988).

[25] G. Raiser, R.J. Clifton, and M. Ortiz, "A New Plate Impact Experiment for Studying Microcracking in Ceramics", *Mechanics of Materials*, 1989, submitted.

Table I. *Materials Used in This Investigation and Their Room Temperature Mechanical and Physical Properties.*

Material	Al_2O_3	Si_3N_4	SiC	Al_2O_3 -25 v/o SiC
Source	Coors Ceramic Golden CO.	Torrington Bearing Co. Torrington CT.	Dow Chemical Co. Midland, MI MI.	Advanced Composites Materials Co. Greer, SC.
Product	AD 998	Noralide	–	Artuff HA9
Specific Gravity	3.90	3.20	3.16	3.74
Ave. Grain Size (μm)	3.0	1.0	4.0	1.0
Young's Mod. (GPa)	345	310	340	393
Poisson's Ratio	0.25	0.26	0.16	0.23
Longitudinal Sound Velocity (m/sec.)	9,400	9,840	10,370	10,250

Table II. *Room Temperature Dynamic and Quasi-Static Fracture Initiation Toughness Values of the Ceramic Materials Tested in the Present Study.*

Material	K_{Id} (MPa$\sqrt{m}$)	K_{Ic} (MPa$\sqrt{m}$)	K_{Id}/K_{Ic}
Al_2O_3	3.5	2.7	1.3
Si_3N_4	3.8	2.8	1.4
SiC	3.3	3.1*	1.1
Al_2O_3–SiC whisker	8.0	5.9	1.4
Al_2O_3† [17]	5.7	4.3	1.3
Al_2O_3–SiC whisker† [17]	7.9	6.6	1.2

†Based on drop-weight impact testing.
*Reported by the supplier.

Table III. *Experimentally Measured Dynamic and Quasi-Static Fracture Initiation Toughness Values of* Al_2O_3 *as a function of Temperature.*

Temp. (°C)	K_{Id} (MPa$\sqrt{m}$)	K_{Ic} (MPa$\sqrt{m}$)	K_{Id}/K_{Ic}
20	3.5	2.7	1.3
900	3.4	2.2	1.5
1100	3.1	2.2	1.4
1300	2.0	1.4	1.4

List of Figures

Fig. 1. A schematic illustration of the room temperature dynamic fracture test specimen.

Fig. 2. A schematic diagram of the experimental set-up for the room temperature dynamic fracture test.

Fig. 3. A schematic diagram of the experimental set-up for the elevated temperature dynamic fracture test.

Fig. 4. Experimentally measured temperature gradient along the length of the ceramic specimen used for dynamic fracture test at 1300°C.

Fig. 5. A schematic diagram of the experimental set-up for the elevated temperature quasi-static fracture test.

Fig. 6. Near-tip finite element mesh used for the numerical analysis of room temperature dynamic fracture test for Al_2O_3.

Fig. 7. Numerical calculations of the pulse at the uncracked ligament and the transmitted pulse at the location of the strain gages as a function of the elapsed time for the room temperature dynamic fracture test on (A) Al_2O_3 and (B) SiC. See text for details.

Fig. 8. Numerical calculations of the ligament pulse and transmitted pulse as a function of the elapsed time for the dynamic fracture test on alumina at (A) 900°C, (B) 1100°C and (C) 1300°C. See text for details.

Fig. 9. Optical micrographs of the fracture surfaces of the room temperature dynamic fracture specimens. (A) Al_2O_3; (B) SiC.

Fig. 10. Scanning electron fractographs of the room temperature dynamic fracture surfaces showing the fatigue pre-crack introduced at the root of the notch under cyclic compression loads. (A) Al_2O_3 and (B) SiC. The crack growth direction is from bottom to top.

Fig. 11. Scanning electron fractographs of Al_2O_3 after dynamic fracture at room temperature. (A) Intergranular failure at the site of dynamic fracture initiation. (B) A higher magnification view of the fracture initiation area.

Fig. 12. Effect of temperature on quasi-static and dynamic fracture initiation toughness of Al_2O_3 in pure tension.

Fig. 13. An optical micrograph of a cross-section of Al_2O_3 subjected to dynamic fracture at 1300°C. Cracking along grain boundaries is evident in the region below the fracture surface (denoted by the dashed line). The tensile axis is vertical.

Fig. 14. Theoretical predictions of the dynamic to static fracture toughness ratio, K_{Id}/K_{Ic}, as a function of microcrack velocity and Poisson's ratio for microcracking brittle solids [24]. Also shown are the results of the present study on room temperature and elevated temperature fracture toughness.

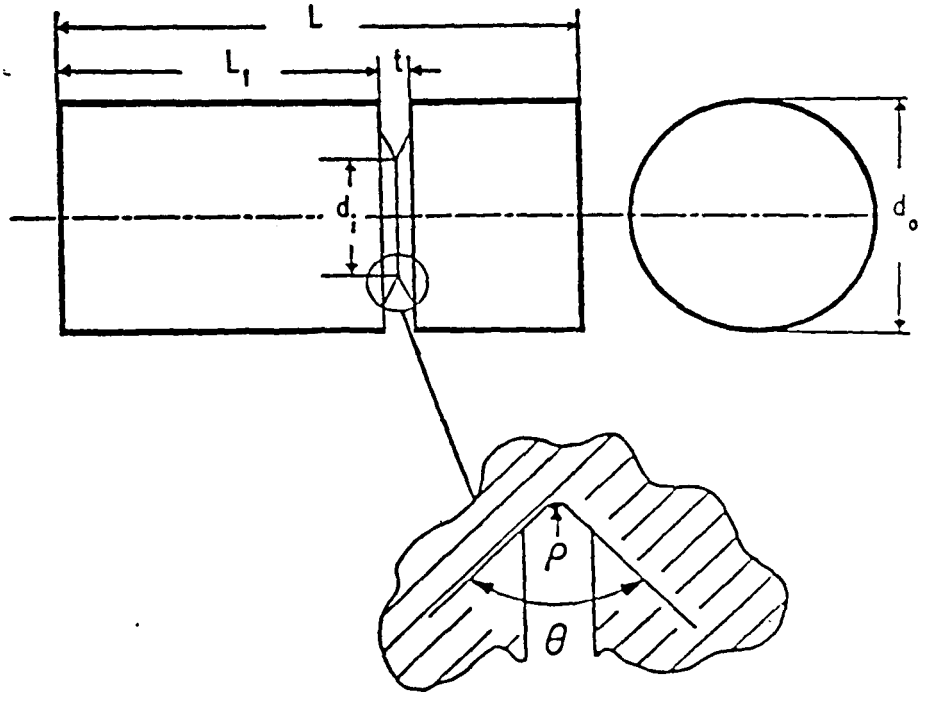

Fig. 1. A schematic illustration of the room temperature dynamic fracture test specimen.

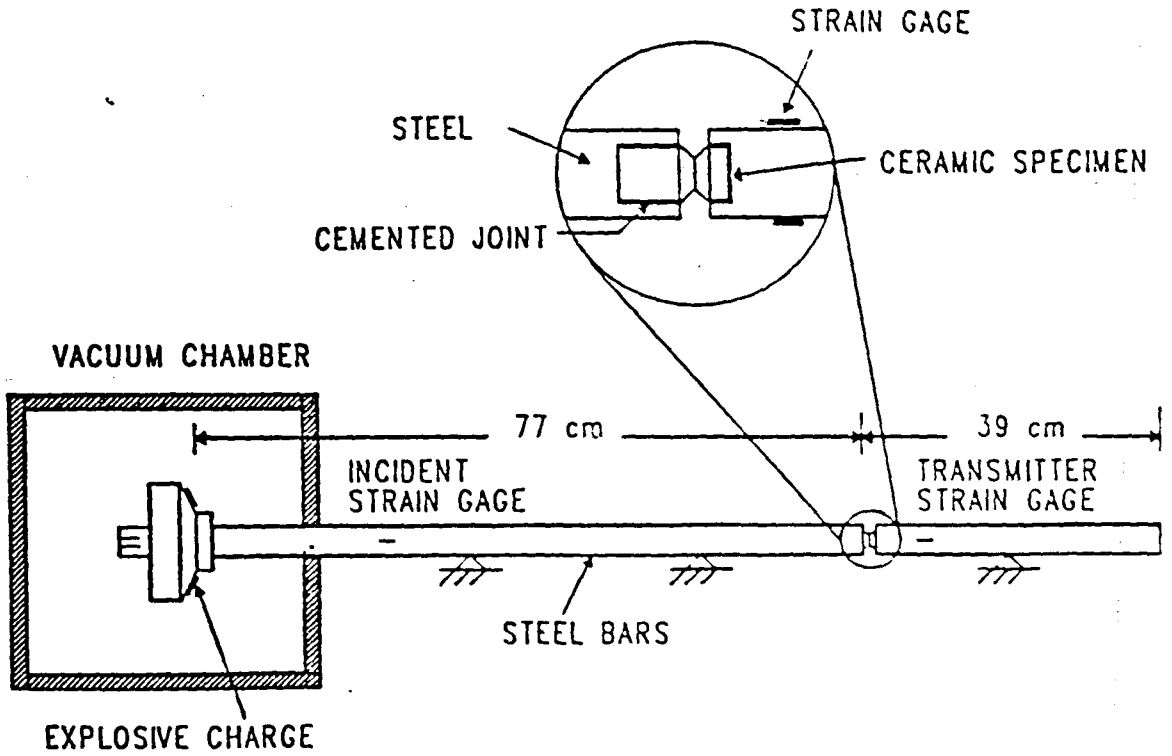

Fig. 2. A schematic diagram of the experimental set-up for the room temperature dynamic fracture test.

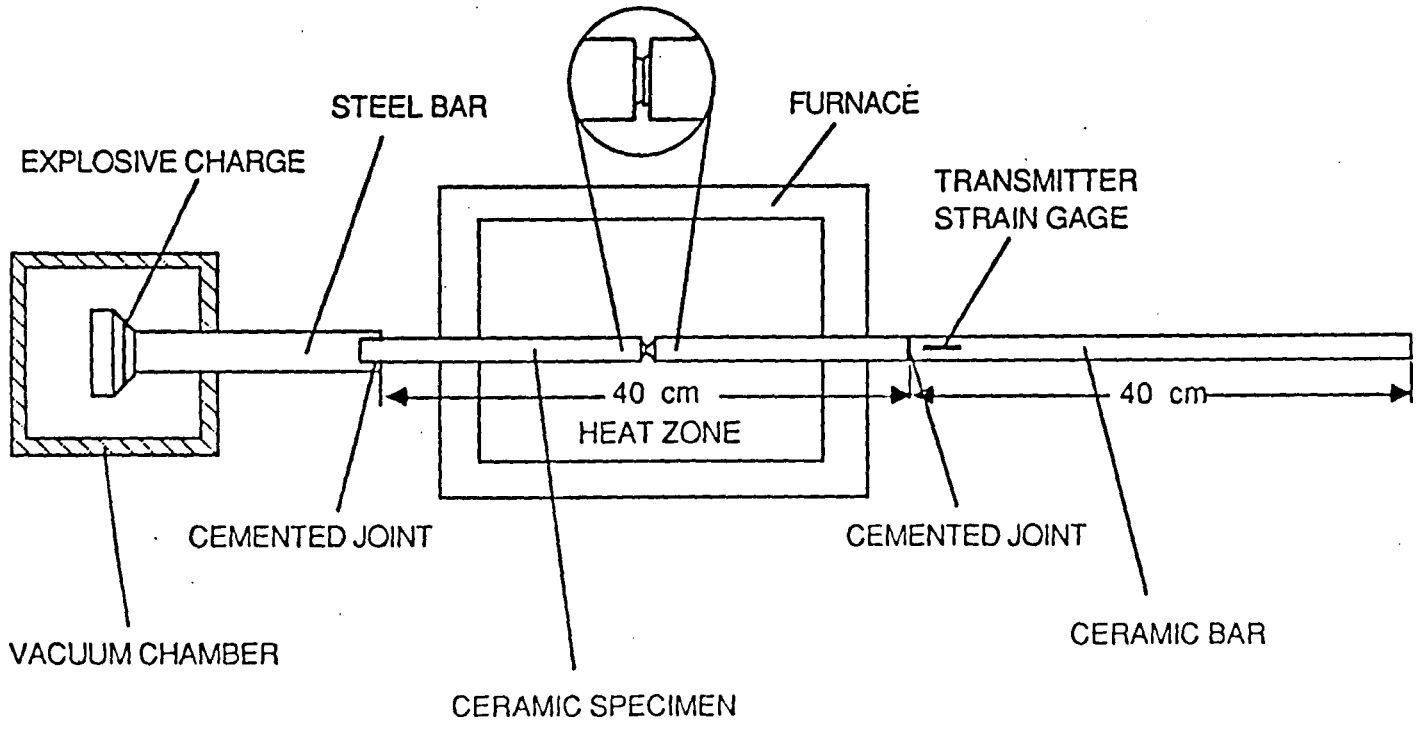

Fig. 3. A schematic diagram of the experimental set-up for the elevated temperature dynamic fracture test.

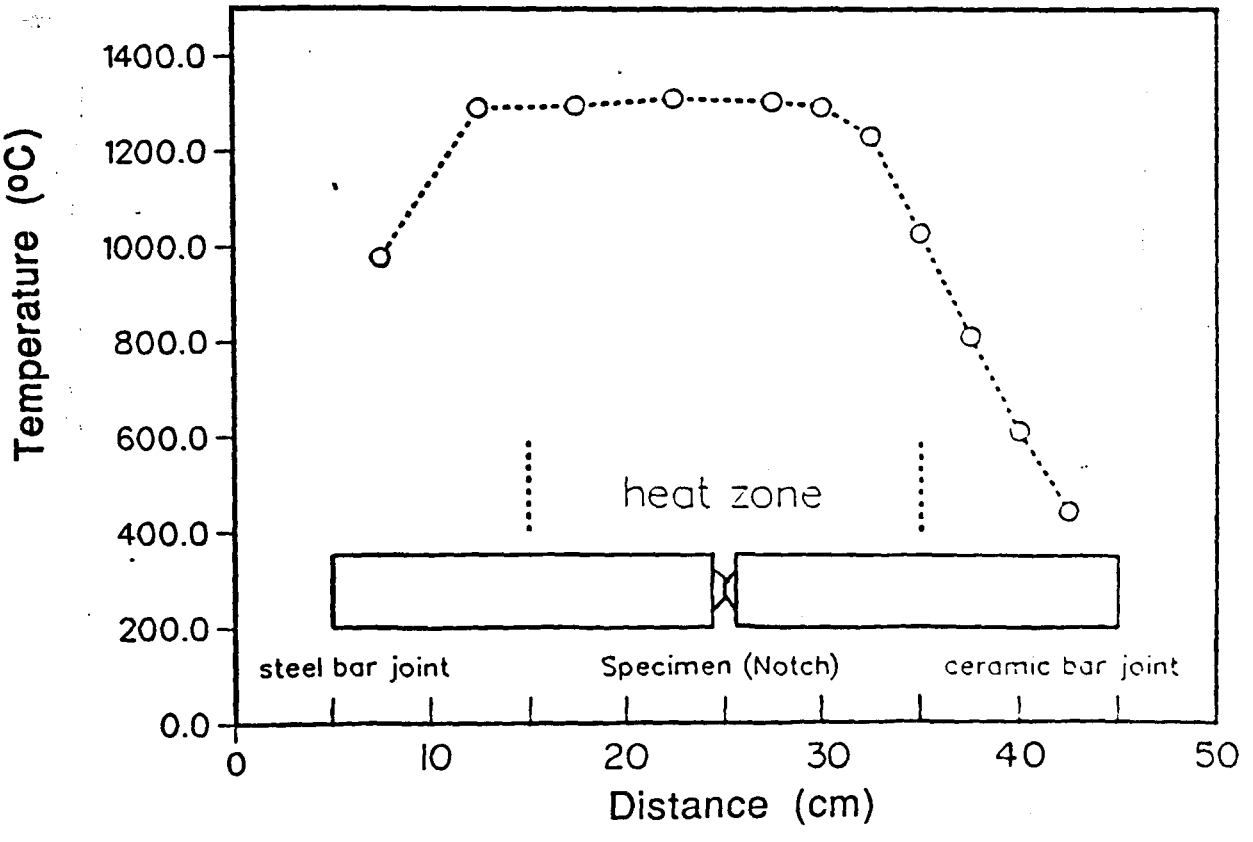

Fig. 4. Experimentally measured temperature gradient along the length of the ceramic specimen used for dynamic fracture test at 1300°C.

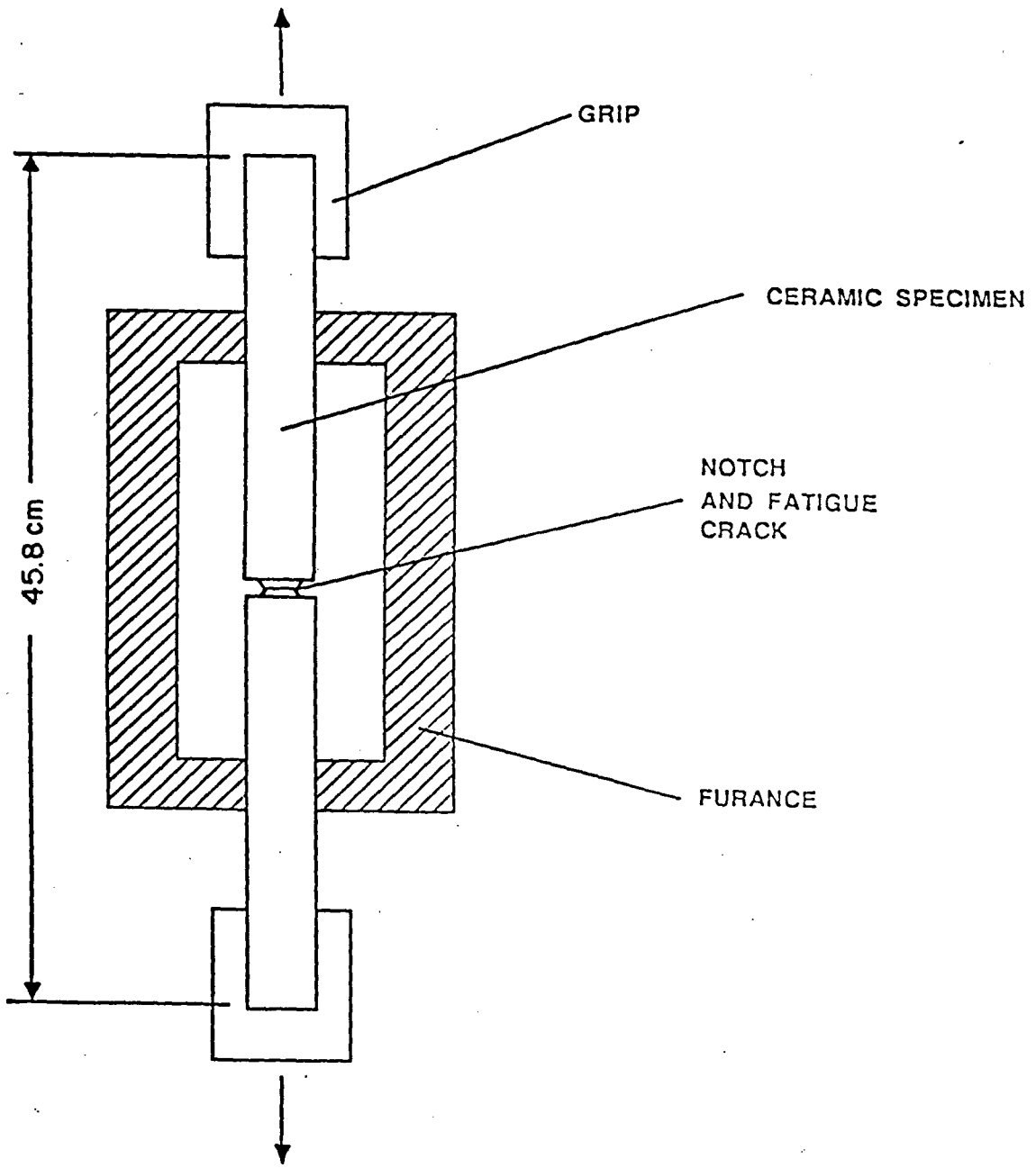

Fig. 5. A schematic diagram of the experimental set-up for the elevated temperature quasi-static fracture test.

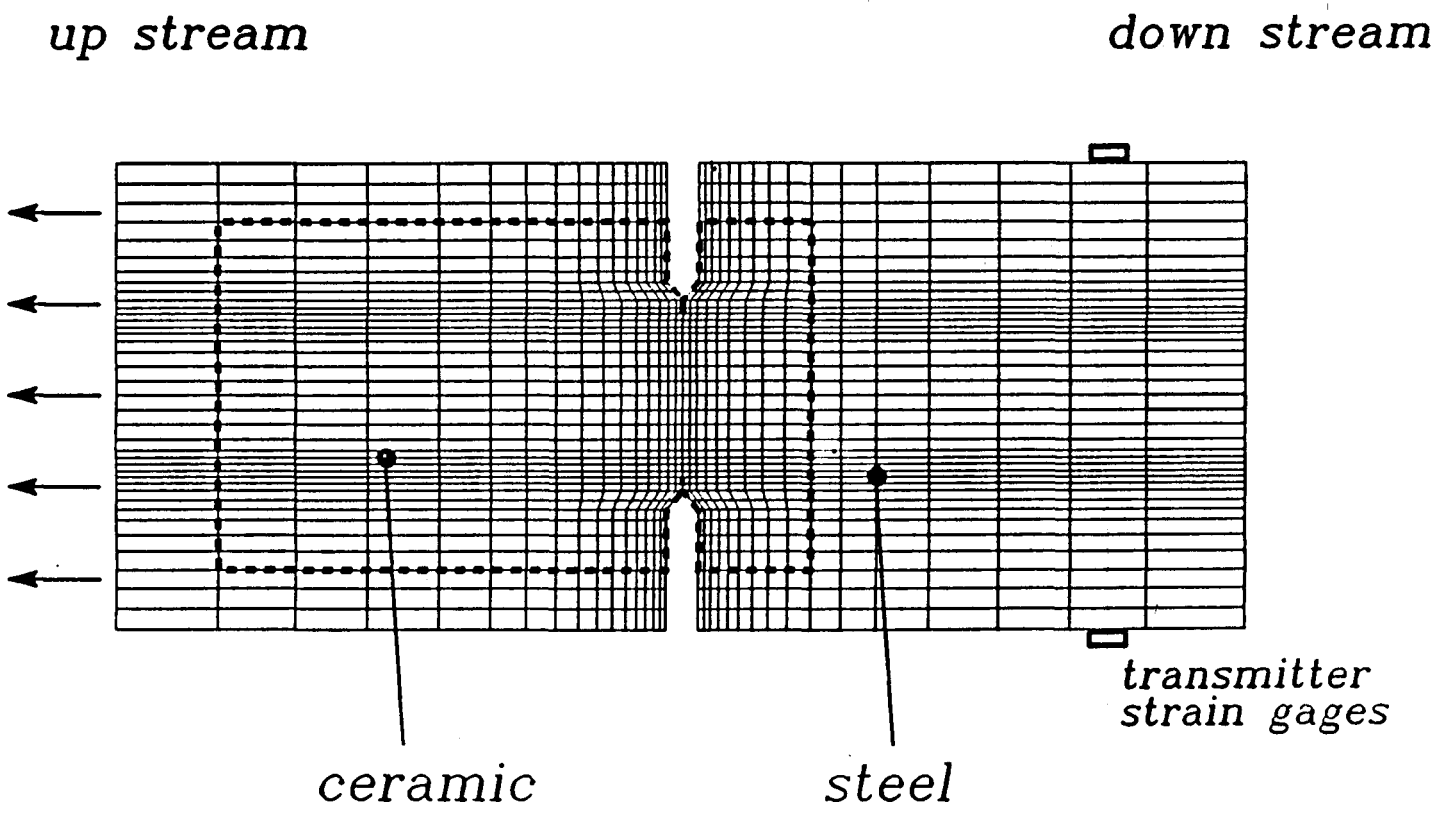

Fig. 6. Near-tip finite element mesh used for the numerical analysis of room temperature dynamic fracture test for Al_2O_3.

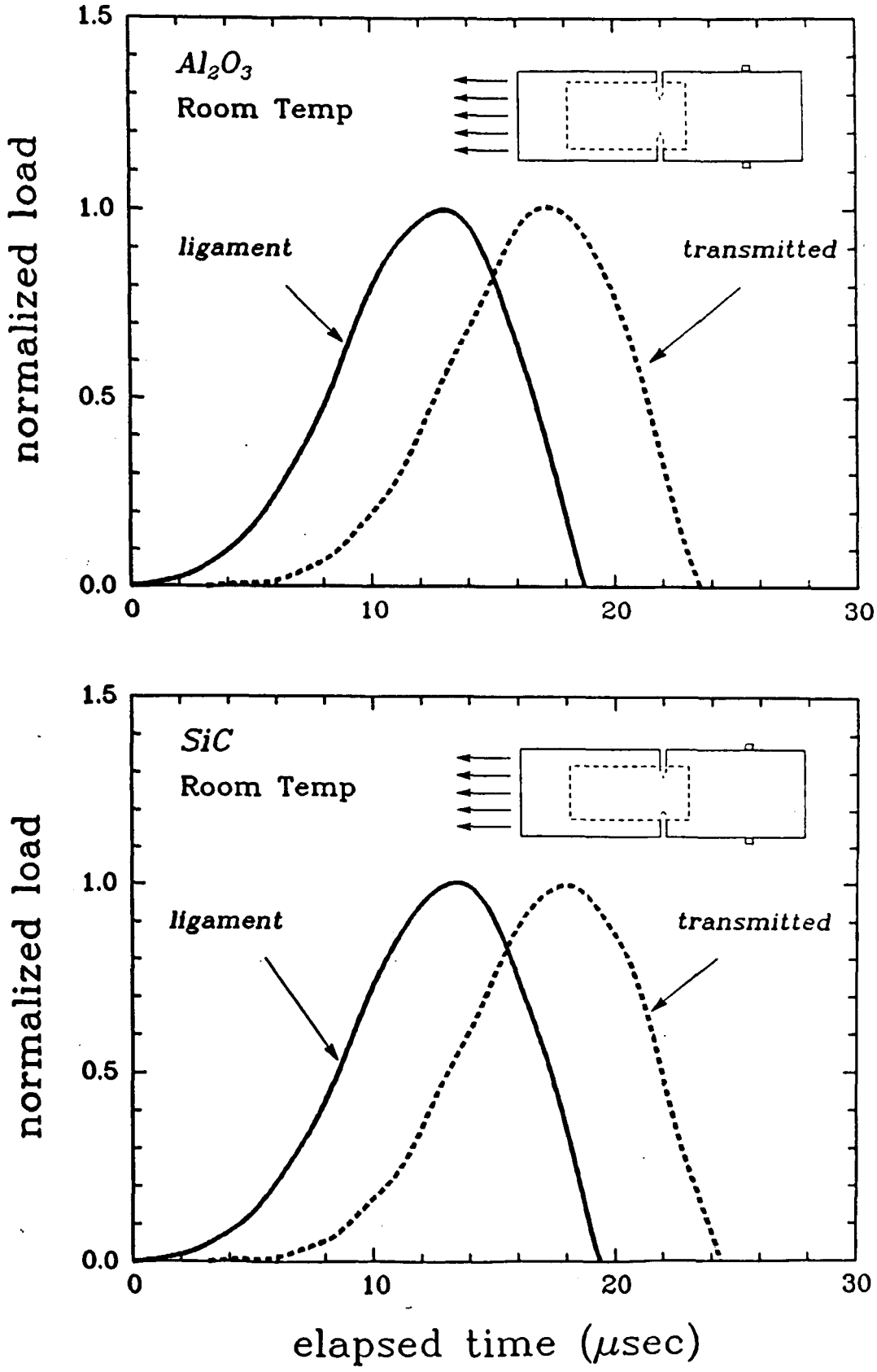

Fig. 7. Numerical calculations of the load at the uncracked ligament and transmitted pulse at the location of the strain gages as a function of the elapsed time for the room temperature dynamic fracture test on (A) Al_2O_3 and (B) SiC. See text for details.

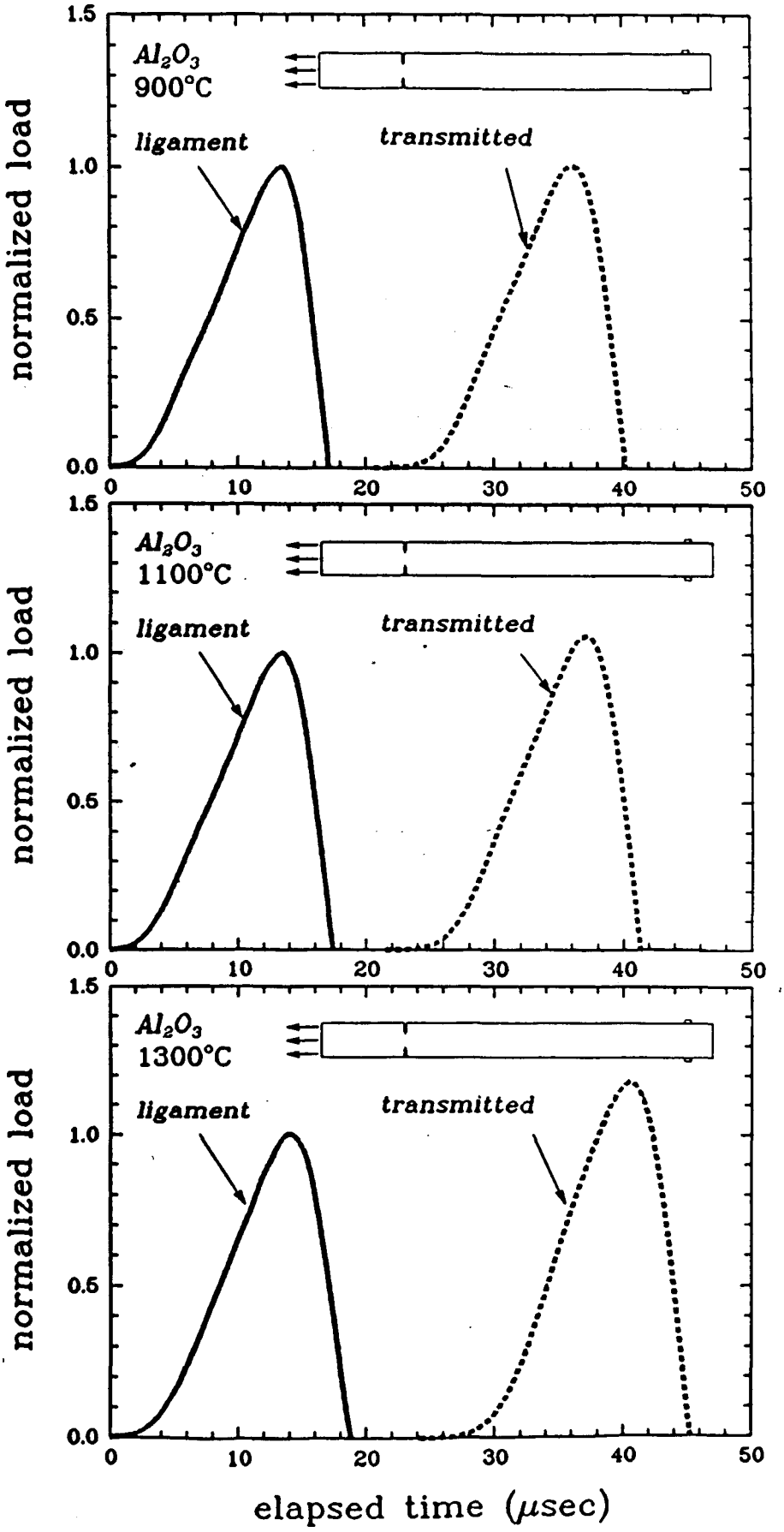

Fig. 8. Numerical calculations of the ligament load and transmitted pulse as a function of the elapsed time for the dynamic fracture test on alumina at (A) 900°C, (B) 1100°C and (C) 1300°C. See text for details.

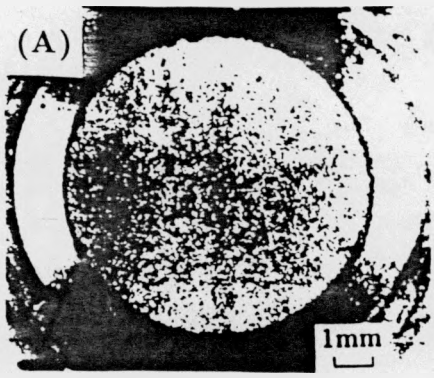

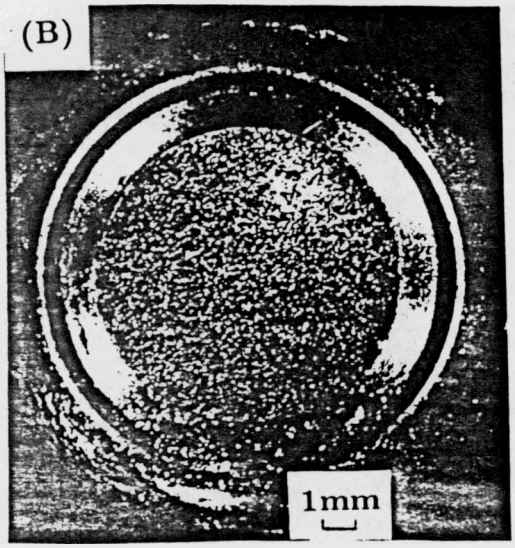

Fig. 9. Optical micrographs of the fracture surfaces of the room temperature dynamic fracture specimens. (A) Al_2O_3; (B) SiC.

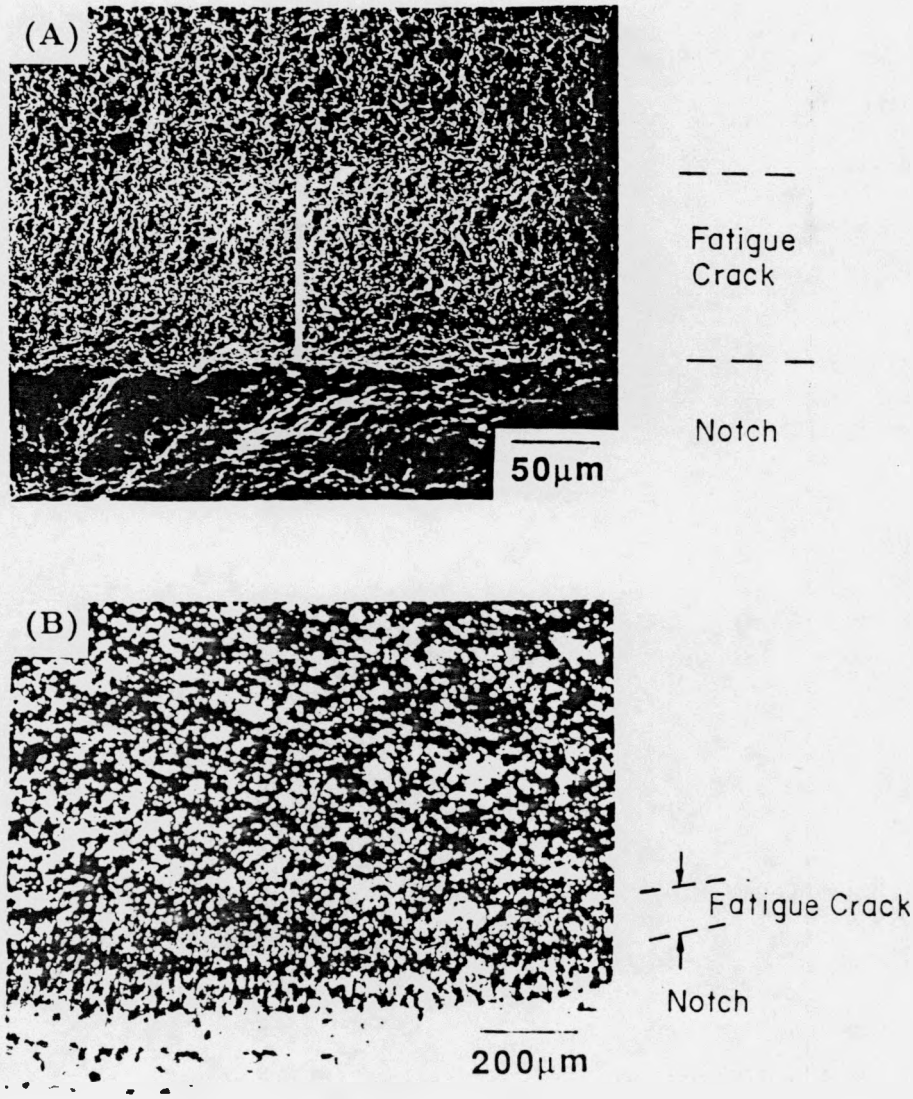

Fig. 10. Scanning electron fractographs of the room temperature dynamic fracture surfaces showing the fatigue pre-crack introduced at the root of the notch under cyclic compression loads. (A) Al_2O_3 and (B) SiC. The crack growth direction is from bottom to top.

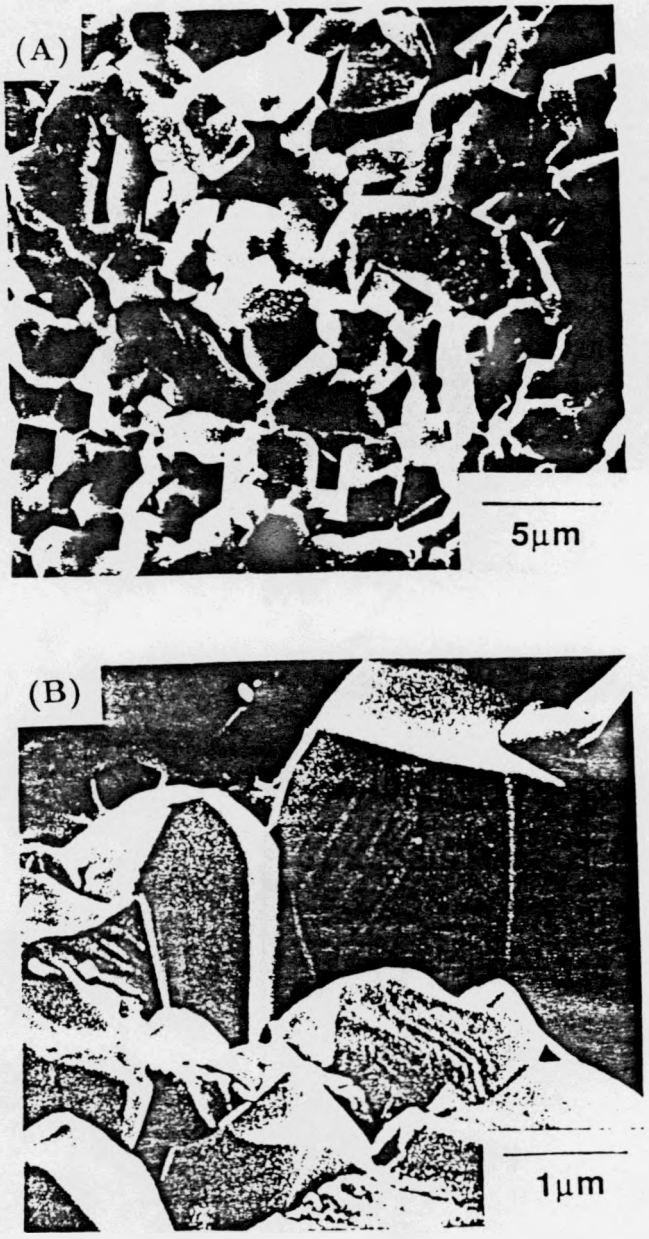

Fig. 11. Scanning electron fractographs of Al_2O_3 which was dynamically fractured at room temperature. (A) Intergranular failure at the site of dynamic fracture initiation. (B) A higher magnification view of the fracture initiation area.

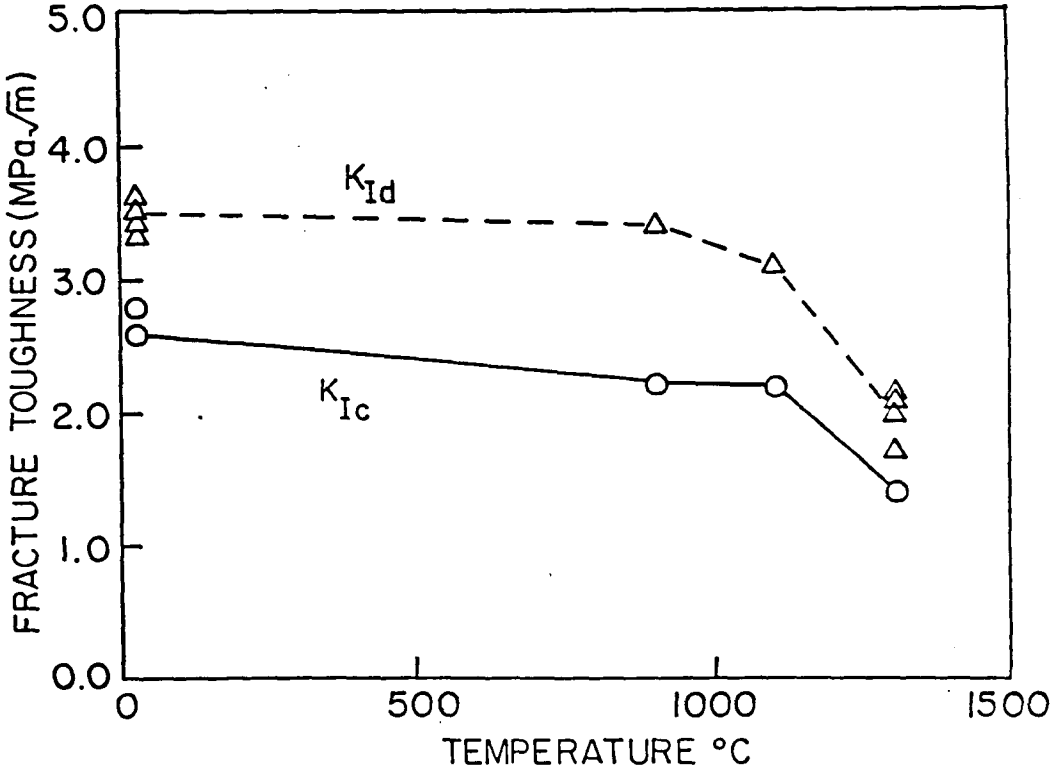

Fig. 12. Effect of temperature on quasi-static and dynamic fracture initiation toughness of Al_2O_3 in pure tension.

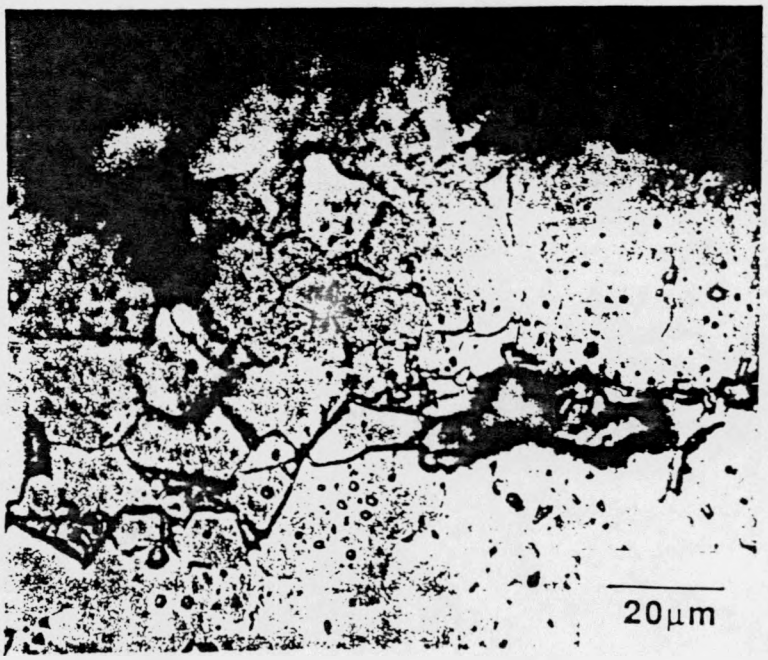

Fig. 13. An optical micrograph of a cross-section of Al_2O_3 subjected to dynamic fracture at 1300°C. Cracking along grain boundaries is evident in the region below the fracture surface (denoted by the dashed line). The tensile axis is vertical.

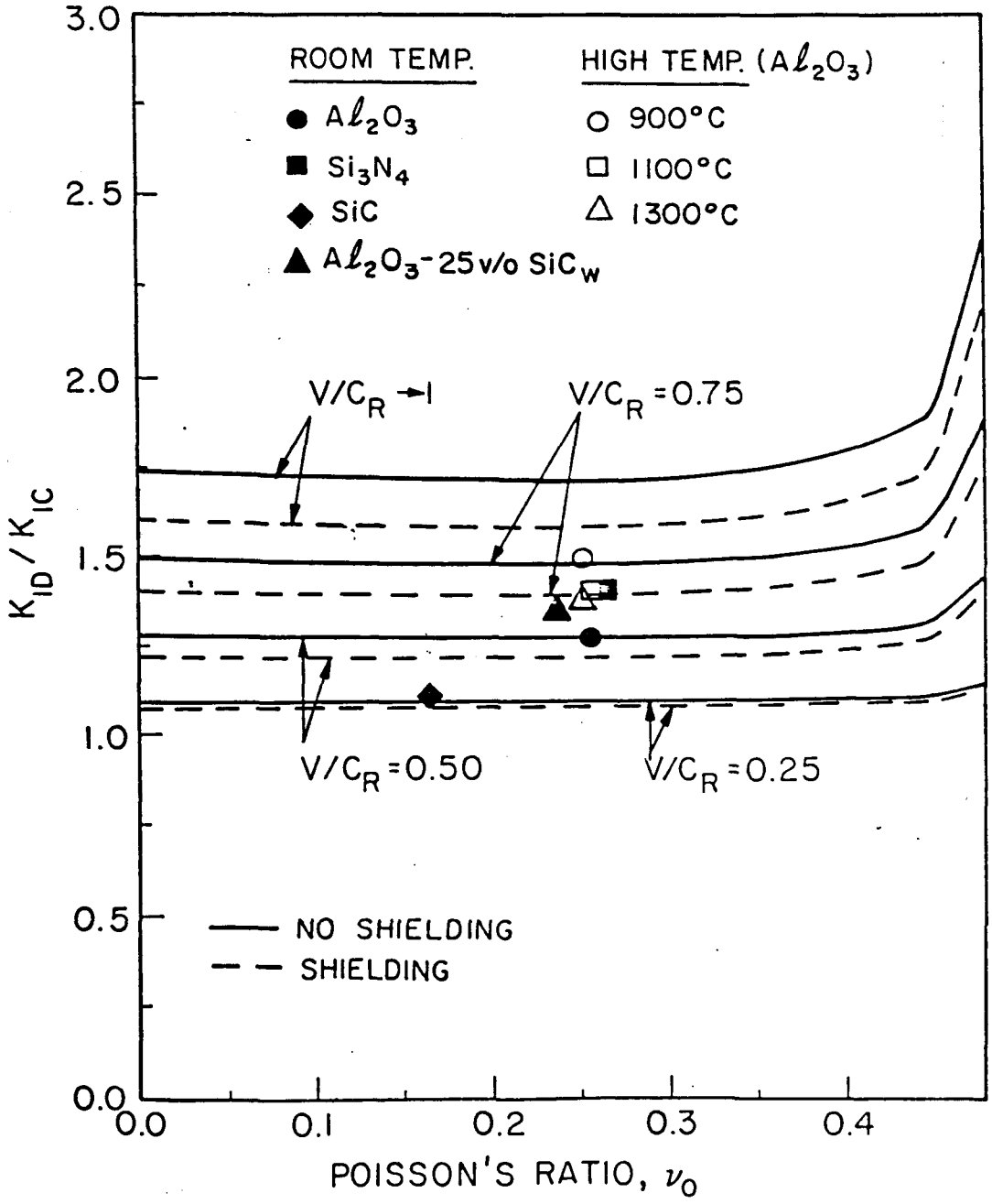

Fig. 14. Theoretical predictions of the dynamic to static fracture toughness ratio, K_{Id}/K_{Ic}, as a function of microcrack velocity and Poisson's ratio for microcracking brittle solids [24]. Also shown are the results of the present study on room temperature and elevated temperature fracture toughness.